

COS-GNN: Continuous Spiking Graph Neural Networks

Nan Yin Mengzhu Wang Li Shen Hitesh Laxmichand Patel Baopu Li Bin Gu Huan Xiong

Abstract

Continuous graph neural networks (CGNNs) have garnered significant attention due to their ability to generalize existing discrete graph neural networks (GNNs) by introducing continuous dynamics. They typically draw inspiration from diffusion-based methods to introduce a novel propagation scheme, which is analyzed using ordinary differential equations (ODE). However, the implementation of CGNNs requires significant computational power, making them challenging to deploy on battery-powered devices. Inspired by recent spiking neural networks (SNNs), which emulate a biological inference process and provide an energy-efficient neural architecture, we incorporate the SNNs with CGNNs in a unified framework, named Continuous Spiking Graph Neural Networks (COS-GNN). We employ SNNs for graph node representation at each time step, which are further integrated into the ODE process along with time. To enhance information preservation and mitigate information loss in SNNs, we introduce the high-order structure of COS-GNN, which utilizes the second-order ODE for spiking representation and continuous propagation. Moreover, we provide the theoretical proof that COS-GNN effectively mitigates the issues of exploding and vanishing gradients, enabling us to capture long-range dependencies between nodes. Experimental results on graph-based learning tasks demonstrate the effectiveness of the proposed COS-GNN over competitive baselines.

1. Introduction

Continuous graph neural networks (CGNNs) play a vital role in shaping modern societies and have been extensively studied across multiple fields in science and engineering, such as social network prediction (Zhang et al., 2022b; Hafiene et al., 2020; Liao et al., 2021), COVID-19 forecasting (Luo et al., 2023), and interacting dynamic system learning (Huang et al., 2021). Typically, CGNNs extend neural ordinary differential equation (ODE) methods to graph neural networks (GNNs) to model the continuous change

of node representations, efficiently addressing dynamic system learning problems (Rusch et al., 2022; Xhonneux et al., 2020). This makes modeling and understanding the intricate dynamics of complex relational systems a major area of research with various applications (Hsieh et al., 2021).

Recently proposed CGNNs (Battaglia et al., 2016; Kipf et al., 2018) approaches typically utilize GNNs to obtain node representations at each timestamp, which are subsequently employed for trend prediction. However, these methods are not able to solve the irregularly sampled issue (Huang et al., 2020; 2021). In contrast, recent ODE works (Poli et al., 2019; Gupta et al., 2022) have proven to be effective in modeling system dynamics when dealing with missing data (Chen et al., 2018). They extend ODE to model interacting dynamical systems, which essentially integrate GNNs with ODE to capture spatio-temporal relationships within dynamical systems. However, for modeling long-term node dependencies, CGNNs tend to consume a substantial amount of energy, posing challenges for their deployment on battery-powered devices.

Inspired by recent work of spiking neural networks (SNNs) (Brette et al., 2007), which transform continuous input into discrete spikes, providing a more intuitive and streamlined approach to inference and model training compared with conventional networks (Zhang et al., 2022a; Maass, 1997), we aim to integrate the energy-efficient attributes of SNNs into CGNNs to confront foundational challenges. However, the combination of SNNs and CGNNs is difficult due to the following challenges: (1) *How to incorporate the SNNs and CGNNs into a unified framework?* SNNs and CGNNs operate by integrating information along two distinct time dimensions: the latency dimension in SNNs and the time dimension in graph-based models. An important challenge is how to amalgamate these dual processes into a unified framework, preserving the energy-efficient characteristics of SNNs while also harnessing the dynamic learning capabilities of CGNNs. (2) *How to alleviate the problem of information loss of SNNs?* SNNs fulfill the need for low-power consumption by discretizing continuous features. However, this binarization process often results in a substantial loss of fine-grained information, leading to diminished performance. Consequently, mitigating the issue of information loss in SNNs represents another significant challenge. (3) *How to guarantee the stability of the proposed*

framework? Traditional graph-based techniques encounter the challenge of exploding and vanishing gradient problems when modeling long-rang dependencies of GNNs. Hence, devising a stable model for graph learning with theoretical guarantee constitutes the third prominent challenge.

To tackle these challenges, we propose a framework named Continuous Spiking Graph Neural Networks (COS-GNN) for graph-based learning tasks. Specifically, to address the first challenge, we approach it by considering SNNs as a type of ODE and integrating it with CGNNs into the partial differential equations (PDE) framework, denoted as COS-GNN-1st. The PDE structure models the initial representation using SNNs by considering the inner time latency at each time step and evaluates the dynamics over time with CGNNs. Furthermore, to address the information loss problem caused by SNNs, we derive a high-order spike representation and introduce the second-order PDE structure, referred to as COS-GNN-2nd. Moreover, we provide empirical evidence that COS-GNN successfully mitigates issues related to exploding and vanishing gradients, enabling the capture of long-range dependencies among nodes. We perform comprehensive evaluations of COS-GNN against state-of-the-art methods on various graph-based datasets, showcasing the efficacy and versatility of proposed approach.

The contributions can be summarized as follows:

- **Novel Architecture.** We incorporate SNNs and CGNNs into a PDE framework, which reserves energy-efficient properties of SNNs while preserving the ability to capture continuous changes in CGNNs. Additionally, we introduce the high-order PDE structure (COS-GNN-2nd), which addresses the information loss challenge encountered in COS-GNN-1st.
- **High-order Spike Representation.** We are the first to derive the second-order spike representation and study the backpropagation of second-order spike ODE to mitigate the information loss problem. This innovation is subsequently applied in the COS-GNN-2nd.
- **Theoretical Analysis.** We provide a theoretical proof demonstrating that COS-GNN effectively mitigates the issue of exploding and vanishing gradients, ensuring the stability of our proposed method.
- **Extensive Experiments.** We evaluate the proposed COS-GNN on extensive graph-based learning datasets, which evaluate that our proposed COS-GNN outperforms the variety of state-of-the-art methods.

2. Related Work

Continuous Graph Neural Networks. Recently, numerous methods based on CGNNs have emerged for modeling dynamic interaction systems (Battaglia et al., 2016; Kipf et al., 2018; Chen et al., 2018). These methods commonly employ

GNNs to initialize node representations at discrete timestamps, which are then utilized for predicting node behaviors. Nevertheless, these discrete methodologies often necessitate the presence of all nodes at each timestamp (Huang et al., 2020; 2021), which is challenging to achieve in real-world scenarios. In contrast, ODE has proven to be effective in modeling system dynamics when dealing with missing data (Chen et al., 2018). Recent works (Poli et al., 2019; Gupta et al., 2022) involve initializing state representations with GNNs, followed by the establishment of a neural ODE model for both nodes and edges, guiding the evolution of the dynamical system. However, CGNNs exhibit substantial energy consumption when modeling long-term node dependencies. In our work, we integrate energy-efficient SNNs into CGNNs, thereby retaining the low energy characteristics of SNNs while harnessing the dynamic learning capabilities of CGNNs.

Spiking Neural Networks. SNNs (Brette et al., 2007; Maass, 1997) have emerged as a promising solution for addressing graph machine learning challenges. Currently, there are two main directions in the field of SNNs. The first direction focuses on establishing a connection between SNNs and Artificial Neural Networks (ANNs), allowing for the conversion from ANNs to SNNs (Rueckauer et al., 2017; Rathi et al., 2020). However, these methods often necessitate a relatively extensive time latency to achieve comparable performance to ANNs, resulting in higher latency and typically increased energy consumption. The second involves the direct training of SNNs using backpropagation techniques (Bohte et al., 2000; Esser et al., 2015; Bellec et al., 2018). These approaches follow the backpropagation through time (BPTT) framework, offering reduced latency but demanding substantial training memory. Nevertheless, there is a scarcity of research concentrating on dynamic spiking graphs, and the solitary existing work (Li et al., 2023) merely integrates SNNs into dynamic graphs, falling short in effectively capturing the continuous changes and subtle dynamics inherent in time series data. Our approach ingeniously combines SNNs with CGNNs to effectively capture the continuous changes and subtle dynamics within graph time series data.

3. Preliminaries

3.1. Continuous Graph Neural Networks

Given a graph $G = (\mathcal{V}, \mathcal{E})$ with the node set \mathcal{V} and the edge set \mathcal{E} . $\mathbf{X} \in \mathbb{R}^{|\mathcal{V}| \times d}$ is the node feature matrix, d is the feature dimension. The binary adjacency matrix denoted as $\mathbf{A} \in \mathbb{R}^{|\mathcal{V}| \times |\mathcal{V}|}$, where $a_{ij} = 1$ denotes there exists a connection between node i and j , and vice versa. Our goal is to learn a node representation \mathbf{H} for downstairs tasks.

First-order CGNNs. The first graph ODE-based CGNN

method is proposed by (Xhonneux et al., 2020). Considering the Simple GNN (Wu et al., 2019) with $\mathbf{H}_{n+1} = \mathbf{A}\mathbf{H}_n + \mathbf{H}_0$, the solution of the ODE is given by:

$$\begin{aligned} \frac{d\mathbf{H}(t)}{dt} &= \ln \mathbf{A} \mathbf{H}(t) + \mathbf{E}, \\ \mathbf{H}(t) &= (\mathbf{A} - \mathbf{I})^{-1} (e^{(\mathbf{A}-\mathbf{I})t} - \mathbf{I}) \mathbf{E} + e^{(\mathbf{A}-\mathbf{I})t} \mathbf{E}, \end{aligned} \quad (1)$$

where $\mathbf{E} = \varepsilon(X)$ is the output of the encoder ε and the initial value $\mathbf{H}(0) = (\ln \mathbf{A})^{-1} (\mathbf{A} - \mathbf{I}) \mathbf{E}$.

Second-order CGNNs. To model high-order correlations in long-term temporal trends, (Rusch et al., 2022) first propose the second-order graph ODE, which is represented as:

$$\mathbf{X}'' = \sigma(\mathbf{F}_\theta(\mathbf{X}, t)) - \gamma \mathbf{X} - \alpha \mathbf{X}', \quad (2)$$

where $(\mathbf{F}_\theta(\mathbf{X}, t))_i = \mathbf{F}_\theta(\mathbf{X}_i(t), \mathbf{X}_j(t), t)$ is a learnable coupling function with parameters θ . Due to the unavailability of an analytical solution for Eqn. 2, GraphCON (Rusch et al., 2022) addresses it through an iterative numerical solver employing a suitable time discretization method. GraphCON utilizes the IMEX (implicit-explicit) time-stepping scheme, an extension of the symplectic Euler method (Hairer et al., 1993) that accommodates systems with an additional damping term.

$$\begin{aligned} \mathbf{Y}^n &= \mathbf{Y}^{n-1} + \Delta t [\sigma(\mathbf{F}_\theta(\mathbf{X}^{n-1}, t^{n-1})) \\ &\quad - \gamma \mathbf{Y}^{n-1} - \alpha \mathbf{Y}^{n-1}], \\ \mathbf{X}^n &= \mathbf{X}^{n-1} + \Delta t \mathbf{Y}^n, \quad n = 1, \dots, N, \end{aligned} \quad (3)$$

where $\Delta t > 0$ is a fixed time-step and \mathbf{Y}^n , \mathbf{X}^n denote the hidden node features at time $t^n = n\Delta t$.

3.2. Spiking Neural Networks

First-order SNNs. In contrast to traditional artificial neural networks, SNNs convert input data into binary spikes over time, with each neuron in the SNNs maintaining a membrane potential that accumulates input spikes. A spike is produced as an output when the membrane potential exceeds a threshold. And the first-order SNNs is formulated as:

$$\begin{aligned} u_{\tau+1,i} &= \lambda(u_{\tau,i} - V_{th} s_{\tau,i}) + \sum_j w_{ij} s_{\tau,j} + b, \\ s_{\tau+1,i} &= \mathbb{H}(u_{\tau+1,i} - V_{th}), \end{aligned} \quad (4)$$

where $\mathbb{H}(x)$ is the Heaviside step function, which is the non-differentiable spiking function. $s_{\tau,i}$ is the binary spike train of neuron i , and λ is the constant. w_{ij} and b are the weights and bias of each neuron.

Second-order SNNs. The first-order neuron models assume that an input voltage spike causes an immediate change in synaptic current, affecting the membrane potential. However, in reality, a spike leads to the gradual release of neurotransmitters from the pre-synaptic neuron to the post-synaptic neuron. To capture the temporal dynamics, we

utilize the synaptic conductance-based LIF model, which considers the gradual changes in input current over time. To solve this, (Eshraghian et al., 2023) propose the second-order SNN, which is formulated as:

$$\begin{cases} I_{\tau+1} = \alpha I_\tau + W X_{\tau+1}, \\ u_{\tau+1,i} = \beta u_{\tau,i} + I_{\tau+1,i} - R, \\ s_{\tau,i} = \mathbb{H}(u_{\tau+1,i} - V_{th}), \end{cases} \quad (5)$$

where $\alpha = \exp(-\Delta t/\tau_{syn})$ and $\beta = \exp(-\Delta t/\tau_{mem})$, τ_{syn} models the time constant of the synaptic current in an analogous way to how τ_{mem} models the time constant of the membrane potential.

4. Methodology

In this part, we present the proposed COS-GNN for modeling the continuous spiking graph neural networks. COS-GNN combines SNNs with CGNNs in a framework of PDE, which preserves the advantage of SNNs and CGNNs simultaneously. To mitigate the problem of information loss attributed to SNNs, we involve the derivation of second-order spike representation and differentiation for second-order SNNs, and then introduce the high-order PDE, referred to as COS-GNN-2nd. Finally, we present a theoretical proof to ensure that our proposed COS-GNN effectively mitigates the challenges associated with gradient exploding and vanishing. The framework of COS-GNN is shown in Figure 1.

4.1. First-order COS-GNN

Specifically, SNNs propagate information within the time latency τ , and the CGNNs evaluate the feature evolution along with time t . We propose the first-order COS-GNN to incorporate SNNs with CGNNs in the form of PDE with their respective timelines. Intuitively, information is interactively propagated in dual time dimensions by both the SNNs and the CGNNs, which is formulated as:

Proposition 4.1. Define the first-order SNNs as $\frac{du_t^\tau}{d\tau} = g(u_t^\tau, \tau)$, and first-order CGNNs as $\frac{du_t^\tau}{dt} = f(u_t^\tau, t)$, then the first-order COS-GNN can be formulated as:

$$\begin{aligned} u_T^N &= 2 \int_0^{T-1} f \left(\int_0^N g(u_y^x, x) dx \right) dy \\ &\quad + \int_{T-1}^T f \left(\int_0^N g(u_y^x, x) dx \right) dy, \end{aligned} \quad (6)$$

or:

$$\begin{aligned} u_T^N &= 2 \int_0^N g \left(\int_0^{T-1} f(u_y^x, x) dy \right) dx \\ &\quad + \int_{T-1}^T f \left(\int_0^N g(u_y^x, x) dx \right) dy. \end{aligned} \quad (7)$$

where N is the total latency of SNNs, and T is the time step length of CGNNs, u_y^x denotes the neuron membrane

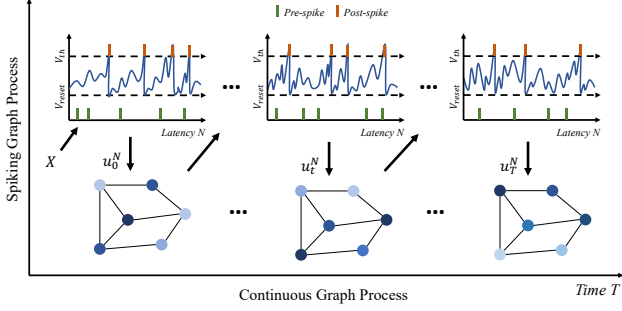


Figure 1. Overview of the proposed COS-GNN. The proposed COS-GNN takes a graph with node features as input, which are initially encoded using the SNNs (first-order or second-order). Subsequently, a first-order or second-order continuous graph process is employed to evolve the representation over different time step. Finally, the representation is projected for downstream tasks.

on latency $x \in [0, N]$ and time step $y \in [0, T]$. Details of derivation are shown in Appendix A.

To provide a comprehensive understanding of Proposition 4.1, we approach it from two distinct perspectives. First, in Eqn. 6, within the temporal dimension where $0 \leq t \leq T$, the SNNs initially compute spike representations at each time step t . These representations are then employed in the evolution of the CGNNs process. Second, as outlined in Eqn. 7, we focus to the latency dimension τ with $0 \leq \tau \leq N$. Then, the CGNNs model the evolution of node embeddings along a time series t and subsequently integrate them across the latency dimension.

In our implementation of the first-order COS-GNN, we employ Eqn. 6 by initially calculating spike representations at each time step, followed by modeling the evolution of node embeddings. As described in (Meng et al., 2022), the first-order spike representation at time step t is denoted as:

$$\mathbf{H}(t) = \frac{\sum_{\tau=1}^N \lambda^{N-\tau} s_\tau^t}{\sum_{\tau=1}^N \lambda^{N-\tau}}. \text{ By combining Eqn. 1, we have:}$$

$$\frac{d\mathbf{H}(t)}{dt} = \ln \mathbf{A} \mathbf{H}(t) + \frac{\sum_{\tau=1}^N \lambda^{N-\tau} s_\tau^0}{\sum_{\tau=1}^N \lambda^{N-\tau}}, \quad (8)$$

where s_τ^t is the binary spike on latency τ and time step t , and $\lambda = \exp(-\frac{\Delta t}{\kappa})$ with $\Delta t \ll \kappa$, κ is the time constant.

4.2. Second-order Spiking Neural Networks

The proposed first-order COS-GNN effectively addresses the challenge of combining SNNs with CGNNs to achieve energy-efficient modeling for continuous graph learning. However, the first-order SNNs typically suffer from the information loss issue. Motivated by recent advancements in high-order structure modeling (Luo et al., 2023), which addresses high-order correlations of nodes, we introduce the second-order COS-GNN to tackle the aforementioned issue. In this part, we begin by deriving the second-order

spike representation and investigating the backpropagation of second-order SNNs.

Second-order SNNs Forward Propagation. We set the forward propagation layer of SNNs to L . According to Eq. 5, the spiking dynamics for SNNs can be formulated as:

$$u^i(n) = \beta^i u^i(n-1) + (1 - \beta^i) \frac{V_{th}^{i-1}}{\Delta t} (\alpha^i I^{i-1}(n-1) + \mathbf{W}^i s^{i-1}(n)) - V_{th}^i s^i(n),$$

where $i = 1, \dots, L$ denotes the i -th layer, s^0 and s^i denote the input and output of SNNs. I^i is the input of the i -th layer, $n = 1, \dots, N$ is the time step and N is the latency. $\alpha^i = \exp(-\Delta\tau/\tau_{syn}^i)$, $\beta^i = \exp(-\Delta\tau/\tau_{mem}^i)$ and $0 < \Delta\tau \ll \{\tau_{syn}^i, \tau_{mem}^i\}$.

Second-order Spike Representation. Considering the second-order SNNs model defined by Eqn. 5, we first define the weighted average input current as $\hat{I}(N) = \frac{1}{(\beta-\alpha)^2} \frac{\sum_{n=0}^{N-1} (\beta^{N-n} - \alpha^{N-n}) I_{in}(n)}{\sum_{n=0}^{N-1} (\beta^{N-n} - \alpha^{N-n})}$, and the scaled weighted firing rate as $\hat{a}(N) = \frac{1}{\beta^2} \frac{V_{th} \sum_{n=0}^{N-1} \beta^{N-n} s(n)}{\sum_{n=0}^{N-1} (\beta^{N-n} - \alpha^{N-n}) \Delta\tau}$. Then, we use $\hat{a}(N)$ denote the spike representation of $\{s(n)\}_{n=1}^N$. Similarly to the first-order spike representation (Meng et al., 2022), we directly determine the relationship between $\hat{I}(N)$ and $\hat{a}(N)$ using a differentiable mapping. Specifically, by combining Eqn. 5, we have:

$$\begin{aligned} u(\tau+1) &= \beta u(\tau) + \alpha I_{syn}(\tau) + I_{input}(\tau) - V_{th} s(\tau) \\ &= \beta^2 u(\tau-k+1) + \alpha \sum_{i=0}^{k-1} \beta^i I_{syn}(\tau-i) \\ &\quad + \sum_{i=0}^{k-1} \beta^i (I_{input}(\tau-i) - V_{th} s(\tau-i)). \end{aligned} \quad (9)$$

By summing Eq. 9 over $n = 1$ to N , we have:

$$\begin{aligned} u(N) &= \frac{1}{\beta - \alpha} \sum_{n=0}^{N-1} (\beta^{N-n} - \alpha^{N-n}) I_{in}(n) \\ &\quad - \frac{1}{\beta} \sum_{n=0}^{N-1} \beta^{N-n} V_{th} s(n). \end{aligned} \quad (10)$$

Dividing Eq. 10 by $\Delta\tau \sum_{n=0}^{N-1} (\beta^{N-n} - \alpha^{N-n})$:

$$\begin{aligned} \hat{a}(N) &= \frac{\beta - \alpha}{\beta} \frac{\hat{I}(N)}{\Delta\tau} - \frac{u(N)}{\Delta\tau \beta \sum_{n=0}^{N-1} (\beta^{N-n} - \alpha^{N-n})} \\ &\approx \frac{\tau_{syn} \tau_{mem}}{\tau_{mem} - \tau_{syn}} \hat{I}(N) \\ &\quad - \frac{u(N)}{\Delta\tau \beta \sum_{n=0}^{N-1} (\beta^{N-n} - \alpha^{N-n})}, \end{aligned}$$

since $\lim_{\Delta\tau \rightarrow 0} \frac{1-\alpha/\beta}{\Delta\tau} = \frac{\tau_{syn} \tau_{mem}}{\tau_{mem} - \tau_{syn}}$ and $\Delta\tau \ll \frac{1}{\tau_{syn}} - \frac{1}{\tau_{mem}}$, we can approximate $\frac{\beta-\alpha}{\beta \Delta\tau}$ by $\frac{\tau_{syn} \tau_{mem}}{\tau_{mem} - \tau_{syn}}$. Follow-

ing (Meng et al., 2022), and take $\hat{a}(N) \in [0, \frac{V_{th}}{\Delta\tau}]$ into consideration and assume V_{th} is small, we ignore the term $\frac{u(N)}{\Delta\tau\beta\sum_{n=0}^{N-1}(\beta^{N-n}-\alpha^{N-n})}$, and approximate $\hat{a}(N)$ with:

$$\lim_{N \rightarrow \infty} \hat{a}(N) \approx \text{clamp}\left(\frac{\tau_{syn}\tau_{mem}}{\tau_{mem}-\tau_{syn}}\hat{I}(N), 0, \frac{V_{th}}{\Delta\tau}\right), \quad (11)$$

where $\text{clamp}(x, a, b) = \max(a, \min(x, b))$. During the training of the second-order SNNs, we have Proposition 4.2, which is similar to (Meng et al., 2022), and the detailed derivation is shown in the Appendix B.

Proposition 4.2. Define $\hat{a}^0(N) = \frac{\sum_{n=0}^{N-1} \beta_i^{N-n-2} s^0(n)}{\sum_{n=0}^{N-1} (\beta_i^{N-n} - \alpha_i^{N-n}) \Delta\tau}$ and $\hat{a}^i(N) = \frac{V_{th} \sum_{n=0}^{N-1} \beta_i^{N-n-2} s^i(n)}{\sum_{n=0}^{N-1} (\beta_i^{N-n} - \alpha_i^{N-n}) \Delta\tau}$, $\forall i = 1, \dots, L$, where $\alpha^i = \exp(-\Delta\tau/\tau_{syn}^i)$ and $\beta^i = \exp(-\Delta\tau/\tau_{mem}^i)$. Further, define the differentiable mappings

$$\mathbf{z}^i = \text{clamp}\left(\frac{\tau_{syn}^i \tau_{mem}^i}{\tau_{mem}^i - \tau_{syn}^i} \mathbf{W}^i \mathbf{z}^{i-1}, 0, \frac{V_{th}}{\Delta\tau}\right), i = 1, \dots, L.$$

If $\lim_{N \rightarrow \infty} \hat{a}^i(N) = \mathbf{z}^i$ for $i = 0, 1, \dots, L-1$, then $\hat{a}^{i+1}(N) \approx \mathbf{z}^{i+1}$ when $N \rightarrow \infty$.

Differentiation on Second-order Spike Representation. In this part, we use the spike representation to drive the backpropagation training algorithm for second-order SNNs. With the forward propagation of the i -th layers, we get the output of SNN with $s^i = \{s^i(1), \dots, s^i(N)\}$. We define the spike representation operator $r(s) = \frac{1}{\beta^2} \frac{V_{th} \sum_{n=0}^{N-1} \beta^{N-n-2} s(n)}{\sum_{n=0}^{N-1} (\beta^{N-n} - \alpha^{N-n}) \Delta\tau}$, and get the final output $\mathbf{o}^L = r(s^L)$. For the simple second-order SNN, assuming the loss function as \mathcal{L} , we calculate the gradient $\frac{\partial \mathcal{L}}{\partial \mathbf{W}^i}$ as:

$$\begin{aligned} \frac{\partial \mathcal{L}}{\partial \mathbf{W}^i} &= \frac{\partial \mathcal{L}}{\partial \mathbf{o}^i} \frac{\partial \mathbf{o}^i}{\partial \mathbf{W}^i} = \frac{\partial \mathcal{L}}{\partial \mathbf{o}^{i+1}} \frac{\partial \mathbf{o}^{i+1}}{\partial \mathbf{o}^i} \frac{\partial \mathbf{o}^i}{\partial \mathbf{W}^i}, \\ \mathbf{o}^i &= r(s^i) \approx \text{clamp}\left(\mathbf{W}^i r(s^{i-1}), 0, \frac{V_{th}}{\Delta\tau}\right). \end{aligned} \quad (12)$$

Therefore, we can compute the gradient of second-order SNNs by calculating $\frac{\partial \mathbf{o}^{i+1}}{\partial \mathbf{o}^i}$ and $\frac{\partial \mathbf{o}^i}{\partial \mathbf{W}^i}$ based on Eqn. 12.

4.3. Second-order COS-GNN

Having obtained the second-order spike representation for SNNs, we introduce the second-order COS-GNN. While obtaining an analytical solution for the second-order COS-GNN may not be feasible, we can derive a conclusion similar to Proposition 4.1. The specifics are presented as follows.

Proposition 4.3. Define the second-order SNNs as $\frac{d^2 u_t^\tau}{d\tau^2} + \delta \frac{du_t^\tau}{d\tau} = e(u_t^\tau, \tau)$, and second-order CGNNs as $\frac{d^2 u_t^\tau}{dt^2} +$

$\gamma \frac{du_t^\tau}{dt} = h(u_t^\tau, t)$, then the second-order COS-GNN follows:

$$u_t^\tau = \int_0^T h\left(\int_0^N e(u_t^\tau) d\tau\right) dt = \int_0^N e\left(\int_0^T h(u_t^\tau) dt\right) d\tau, \\ \frac{\partial^2 u_t^\tau}{\partial \tau^2} + \delta \frac{\partial u_t^\tau}{\partial \tau} = g(u_t^\tau), \quad \frac{\partial^2 u_t^\tau}{\partial t^2} + \gamma \frac{\partial u_t^\tau}{\partial t} = f(u_t^\tau),$$

where $e(u_t^\tau) = \int_0^N g(u_t^\tau) d\tau - \delta(u_t^N - u_t^0)$, $h(u_t^\tau) = \int_0^T f(u_t^\tau) dt - \gamma(u_T^\tau - u_0^\tau)$, $\frac{\partial e(u_t^\tau)}{\partial \tau} = g(u_t^\tau)$ and $\frac{\partial h(u_t^\tau)}{\partial t} = f(u_t^\tau)$. δ and γ are the hyperparameters of second-order SNNs and CGNNs.

The details are derived in Appendix C. Similarly to the first-order COS-GNN, we implement the second-order COS-GNN by calculating the spike representation on each time step and then model the node embedding with Eqn. 3. Furthermore, to optimize the second-order COS-GNN, we analyze the differentiation of the second-order COS-GNN. Denote the loss function as $\mathcal{L} = \sum_{i \in \mathcal{V}} |\mathbf{X}_i^N - \bar{\mathbf{X}}_i|^2$, and $\bar{\mathbf{X}}_i$ is the label of node i . With the chain rule, we have: $\frac{\partial \mathcal{L}}{\partial \mathbf{W}^l} = \frac{\partial \mathcal{L}}{\partial \mathbf{o}_T^N} \frac{\partial \mathbf{o}_T^N}{\partial \mathbf{o}_T^l} \frac{\partial \mathbf{o}_T^l}{\partial \mathbf{W}^l}$. From (Rusch et al., 2022), we have the conclusion that the traditional GNN model has the problem of gradient exponentially or vanishing, thus, we study the upper bound of the proposed COS-GNN.

Proposition 4.4. Let \mathbf{X}^n and \mathbf{Y}^n be the node features, generated by Eqn. 3, and $\Delta t \ll 1$. The gradient of the second-order CGNNs \mathbf{W}_l is bounded as Eqn. 13, and the gradient of the second-order SNNs \mathbf{W}^k is bounded as Eqn. 14:

$$\begin{aligned} \left| \frac{\partial \mathcal{L}}{\partial \mathbf{W}_l} \right| &\leq \frac{\beta' \hat{\mathbf{D}} \Delta t (1 + \Gamma T \Delta t)}{v} \left(\max_{1 \leq i \leq v} (|\mathbf{X}_i^0| + |\mathbf{Y}_i^0|) \right) \\ &\quad + \frac{\beta' \hat{\mathbf{D}} \Delta t (1 + \Gamma T \Delta t)}{v} \left(\max_{1 \leq i \leq v} |\bar{\mathbf{X}}_i| + \beta \sqrt{T \Delta t} \right)^2, \end{aligned} \quad (13)$$

$$\begin{aligned} \left| \frac{\partial \mathcal{L}}{\partial \mathbf{W}^k} \right| &\leq \frac{(1 + T \Gamma \Delta t)(1 + N \Theta \Delta \tau) V_{th}}{v \beta^2 \Delta \tau} \left(\max_{1 \leq i \leq v} |\mathbf{X}_i^N| \right. \\ &\quad \left. + \max_{1 \leq i \leq v} |\bar{\mathbf{X}}_i| \right). \end{aligned} \quad (14)$$

where $\beta = \max_x |\sigma(x)|$, $\beta' = \max_x |\sigma'(x)|$, $\hat{\mathbf{D}} = \max_{i,j \in \mathcal{V}} \frac{1}{\sqrt{d_i d_j}}$, and $\Gamma := 6 + 4\beta' \hat{\mathbf{D}} \max_{1 \leq n \leq T} \|\mathbf{W}^n\|_1$, $\Theta := 6 + 4\beta' \hat{\mathbf{D}} \max_{1 \leq n \leq N} \|\mathbf{W}^n\|_1$. d_i is the degree of node i , $\bar{\mathbf{X}}_i$ is the label of node i . Eqn. 13 can be obtained from (Rusch et al., 2022) directly, and the derivation of the Eqn. 14 is presented in Appendix D.

The upper bound in Proposition 4.4 demonstrates that the total gradient remains globally bounded, regardless of the number of CGNNs layers T and SNNs layers N , as long as $\Delta t \sim T^{-1}$ and $\Delta \tau \sim N^{-1}$. This effectively addresses the issues of exploding and vanishing gradients.

5. Experiments

To evaluate the effectiveness of our proposed COS-GNN, we conduct extensive experiments with COS-GNN across various graph learning tasks, including node classification and graph classification. We assess the method in two settings: COS-GNN-1st, using first-order SNNs and second-order CGNNs, and COS-GNN-2nd, employing second-order SNNs and second-order CGNNs.

5.1. Experimental Settings

Datasets. For the node classification, we evaluate COS-GNN on homophilic (i.e., Cora (McCallum et al., 2000), Citeseer (Sen et al., 2008) and Pubmed (Namata et al., 2012)) and heterophilic (i.e., Texas, Wisconsin and Cornell from the WebKB¹) datasets, where high homophily indicates that a node’s features are similar to those of its neighbors, and heterophily suggests the opposite. The homophily level is measured according to (Pei et al., 2020), and is reported in Table 1 and 2. In the graph classification task, we utilize the MNIST dataset (LeCun et al., 1998). To represent the grey-scale images as irregular graphs, we associate each superpixel (large blob of similar color) with a vertex, and the spatial adjacency between superpixels with edges. Each graph consists of a fixed number of 75 superpixels (vertices). To ensure consistent evaluation, we adopt the standard splitting of 55K-5K-10K for training, validation, and testing purposes (Rusch et al., 2022).

Baselines. For the homophilic datasets, we use standard GNN baselines: GCN (Kipf & Welling, 2017), SGC (Wu et al., 2019), GAT (Velickovic et al., 2017), MoNet (Monti et al., 2017), GraphSage (Hamilton et al., 2017), CGNN (Xhonneux et al., 2020), GDE (Poli et al., 2019), GRAND (Chamberlain et al., 2021), GraphCON (Rusch et al., 2022) and SpikingGCN (Zhu et al., 2022). Due to the assumption on neighbor feature similarity does not hold in the heterophilic datasets, we utilize additional specific GNN methods as baselines: GPRGNN (Chien et al., 2020), H2GCN (Zhu et al., 2020), GCNII (Chen et al., 2020), Geom-GCN (Pei et al., 2020) and PairNorm (Zhao & Akoglu, 2019). For the graph classification task, we apply ChebNet (Defferrard et al., 2016), PNCNN (Finzi et al., 2021), SplineCNN (Fey et al., 2018), GIN (Xu et al., 2019), and GatedGCN (Bresson & Laurent, 2017) for comparison.

Implementation Details. For the homophilic node classification task, we report the average results of 20 random initialization across 5 random splits. For the heterophilic node classification task, we present the average performance of the respective model over 10 fixed train/val/test splits. The results of baselines are reported in (Rusch et al., 2022).

¹<http://www.cs.cmu.edu/afs/cs.cmu.edu/project/theo-11/www/wwkb/>

Table 1. The test accuracy (in %) for node classification on homophilic datasets. The results are calculated by averaging the results of 20 random initializations across 5 random splits. The mean and standard deviation of these results are obtained. **Bold** numbers means the best performance, and underline numbers indicates the second best performance.

<i>Homophily level</i>	Cora 0.81	Citeseer 0.74	Pubmed 0.80
GAT-ppr	81.6±0.3	68.5±0.2	76.7±0.3
MoNet	81.3±1.3	71.2±2.0	78.6±2.3
GraphSage-mean	79.2±7.7	71.6±1.9	77.4±2.2
GraphSage-maxpool	76.6±1.9	67.5±2.3	76.1±2.3
CGNN	81.4±1.6	66.9±1.8	66.6±4.4
GDE	78.7±2.2	71.8±1.1	73.9±3.7
GCN	81.5±1.3	71.9±1.9	77.8±2.9
GAT	81.8±1.3	71.4±1.9	78.7±2.3
SGC	81.5±0.4	71.7±0.4	79.2±0.3
GRAND	83.6±1.0	73.4±0.5	78.8±1.7
GraphCON-GCN	81.9±1.7	72.9±2.1	78.8±2.6
GraphCON-GAT	83.2±1.4	73.2±1.8	79.5±1.8
SpikingGCN	80.7±0.6	72.5±0.2	77.6±0.5
COS-GNN-1st	<u>83.3±2.1</u>	<u>73.7±2.0</u>	76.9±2.7
COS-GNN-2nd	83.7±1.3	75.2±2.0	79.6±2.3

For COS-GNN-1st, we set the hyperparameter λ to 1. As for COS-GNN-2nd, we set the hyperparameters α and β to 1 as default. The time latency N in SNNs are set to 8. For all the methods, we set the hidden size to 64 and the learning rate to 0.001 as default.

5.2. Performance Comparision

Homophilic Node Classification. Table 1 shows the results of the proposed COS-GNN with the comparison of baselines. From the results, we find that: (1) Compared with the discrete methods (i.e., the baselines excluding GraphCON), the continuous methods (GraphCON and COS-GNN) achieve the best and second best performance, indicating that the continuous methods would help to capture the continuous changes and subtle dynamics from graphs. (2) COS-GNN-1st and COS-GNN-2nd outperforms other baselines in most cases. We attribute that, even if SNNs loses some detailed information, COS-GNN can still achieve good performance on the relatively simple homophilic dataset. Furthermore, the application of SNNs contributes to improved efficiency in the COS-GNN framework. (3) COS-GNN-2nd consistently outperforms the COS-GNN-1st. This highlights the significance of introducing high-order structures to preserve information and mitigates the information loss issue caused by first-order SNNs. Although high-order structures suffer higher energy costs compared to first-order, the performance gains make it worthwhile to deploy them. (4) COS-GNN-1st and COS-GNN-2nd outperforms the spiking-based method (i.e., Spiking) in most case. This can be attributed to the utilization of CGNNs, which efficiently capture the spatio-

Table 2. The test accuracy (in %) for node classification on heterophilic datasets. All results represent the average performance of the respective model over 10 fixed train/val/test splits. **Bold** numbers means the best performance, and underline numbers indicates the second best performance.

<i>Homophily level</i>	Texas	Wisconsin	Cornell
	0.11	0.21	0.30
GPRGNN	78.4±4.4	82.9±4.2	80.3±8.1
H2GCN	84.9±7.2	87.7±5.0	82.7±5.3
GCNII	77.6±3.8	80.4±3.4	77.9±3.8
Geom-GCN	66.8±2.7	64.5±3.7	60.5±3.7
PairNorm	60.3±4.3	48.4±6.1	58.9±3.2
GraphSAGE	82.4±6.1	81.2±5.6	76.0±5.0
MLP	80.8±4.8	85.3±3.3	81.9±6.4
GCN	55.1±5.2	51.8±3.1	60.5±5.3
GAT	52.2±6.6	49.4±4.1	61.9±5.1
GraphCON-GCN	<u>85.4±4.2</u>	<u>87.8±3.3</u>	84.3±4.8
GraphCON-GAT	82.2±4.7	85.7±3.6	83.2±7.0
COS-GNN-1st	81.6±6.2	84.9±3.2	80.4±1.9
COS-GNN-2nd	87.3±4.2	88.8±2.5	<u>83.7±2.7</u>

temporal relationships within dynamical systems.

Heterophilic Node Classification. Table 2 shows the results of heterophilic node classification, and we observe that: (1) The traditional message-passing-based methods (GCN, GAT, GraphSAGE and Geom-GCN) perform worse than the well-designed methods (GPRGNN, H2GCN, GCNII, GraphCON and COS-GNN) for heterophilic datasets. This disparity comes from the inaccurate assumption of neighbor feature similarity, which doesn't hold in heterophilic datasets. The propagation of heterophilic information between nodes would degrade the model's representation ability, leading to a decline in performance. (2) The COS-GNN-1st performs less effectively than GraphCON. This is because node prediction tasks on heterophilic datasets are more influenced by the characteristics of heterophilic features compared to homophilic datasets. Consequently, the information loss issue caused by first-order SNNs results in worse model performance. (3) The COS-GNN-2nd consistently outperforms COS-GNN-1st, providing further evidence of the effectiveness of high-order structures in preserving information and mitigating the issue of information loss.

Graph Classification. We present the graph classification results of our proposed COS-GNN alongside comparison baselines in Table 3. From Table 3, we find that: (1) In the graph classification tasks, CGNNs methods (i.e., COS-GNN and GraphCON) consistently outperform the baseline methods across all cases. This underscores the importance of employing a continuous processing approach when dealing with graph data, enabling the extraction of continuous changes and subtle dynamics from graphs. (2) The COS-GNN-1st performs worse than the COS-GNN-2nd, highlighting the significance of incorporating high-order

Table 3. The test accuracy (in %) for graph classification on MNIST datasets. **Bold** numbers means the best performance, and underline numbers indicates the second best performance.

Model	Test accuracy
ChebNet (Defferrard et al., 2016)	75.62
MoNet (Monti et al., 2017)	91.11
PNCNN (Finzi et al., 2021)	98.76
SplineCNN (Fey et al., 2018)	95.22
GIN (Xu et al., 2019)	97.23
GatedGCN (Bresson & Laurent, 2017)	97.95
GCN (Kipf & Welling, 2017)	88.89
GAT (Velickovic et al., 2017)	96.19
GraphCON-GCN (Rusch et al., 2022)	98.68
GraphCON-GAT (Rusch et al., 2022)	98.91
COS-GNN-1st	98.82
COS-GNN-2nd	98.92

structures to obtain additional information for prediction, without incurring significant overhead. (3) The COS-GNN-1st performs worse than GraphCON-GAT and better than GraphCON-GCN. Compared to GraphCON-GCN, the information loss caused by SNNs does not critically affect graph representation ability. On the contrary, the binarization operation of SNNs contributes to reduced energy consumption. Graph-GAT outperforms COS-GNN-1st, mainly because the GAT method enhances graph representation. However, Graph-GAT still lags behind COS-GNN-2nd, indicating that the introduction of high-order structures mitigates the information loss issue associated with first-order methods.

5.3. Ablation Study

We conducted ablation studies to assess the contributions of different components using two variants, and the results are presented in Table 4. Specifically, we introduced two model variants: (1) COS-GNN-1st-2nd, which utilizes the first-order SNNs and second-order CGNNs, and (2) COS-GNN-2nd-1st, incorporating the second-order SNNs and first-order CGNNs. Table 4 shows that (1) COS-GNN-2nd consistently outperforms other variations, while COS-GNN-1st-2nd yields the worst performance. This is because the issue of information loss is crucial for graph representation, and the incorporation of high-order SNNs assists in preserving more information, consequently achieving superior results. (2) In most cases, COS-GNN-2nd-1st outperforms both COS-GNN-1st and COS-GNN-1st-2nd, suggesting that, compared to the capability of CGNNs in capturing dynamic node relationships, the ability to mitigate the issue of information loss is more important.

Table 4. Ablation results. **Bold** numbers means the best performance.

<i>Homophily level</i>	Cora	Citeseer	Pubmed	Texax	Wisconsin	Cornell	Avg.
	0.81	0.74	0.80	0.11	0.21	0.3	
COS-GNN-1st-2nd	83.2 \pm 1.4	74.1 \pm 1.4	76.3 \pm 2.2	81.7 \pm 3.9	85.1 \pm 2.8	81.0 \pm 1.9	80.2
COS-GNN-2nd-1st	83.5 \pm 1.8	73.4 \pm 2.1	77.2 \pm 2.3	83.1 \pm 3.8	84.4 \pm 2.2	81.2 \pm 2.7	80.5
COS-GNN-1st	83.3 \pm 2.1	73.7 \pm 2.0	76.9 \pm 2.7	81.6 \pm 6.2	84.9 \pm 3.2	80.4 \pm 1.9	80.1
COS-GNN-2nd	83.7\pm1.3	75.2\pm2.0	79.6\pm2.3	87.3\pm4.2	88.8\pm2.5	83.7\pm2.7	83.1

Table 5. Operations comparison on different datasets.

models	Cora	Citeseer	Pubmed
GCN	67.77K	79.54K	414.16K
GAT	308.94K	349.91K	1.53M
SGC	10.03K	22.22K	1.50K
COS-GNN-1st	2.33K	1.94K	1.02K
COS-GNN-2nd	3.97K	3.42K	2.78K

5.4. Energy Efficiency Analysis

To evaluate the energy efficiency of COS-GNN, we apply the metric in (Zhu et al., 2022), which quantifies the number of operations needed for node prediction. The results are reported in Table 5. From the results, we find that the COS-GNN-1st and COS-GNN-2nd have a significant operation reduction compared with baselines. The conventional operation unit for ANNs on GPUs is commonly configured as multiply-accumulate (MAC), whereas for SNNs on neuromorphic chips, it takes the form of synaptic operation (SOP). The SOP is defined as the change in membrane potential in the LIF nodes. According to (Hu et al., 2021; Kim et al., 2020), the SOP of SNNs consumes significantly less energy than the MAC in ANNs, which further underscores the energy efficiency of COS-GNN.

5.5. Sensitivity Analysis

In this part, we examine the sensitivity of the proposed COS-GNN to its hyperparameters, specifically the time latency parameter (N) in SNNs, which plays a crucial role in the model’s performance. N controls the number of SNNs propagation steps and is directly related to the training complexity. Figure 2 shows the results of N across different datasets. We initially vary the parameter N within the range of $\{5, 6, 7, 8, 9, 10, 11\}$ while keeping other parameters fixed. From the results, we find that, the performance exhibits a increasing trend initially, followed by stabilization as the value of N increases. Typically, in SNNs, spiking signals are integrated with historical information at each time latency. Smaller values of N result in less information available for graph representation, degrading the performance. However, large values of N increase model complexity during training. Striking a balance between model performance

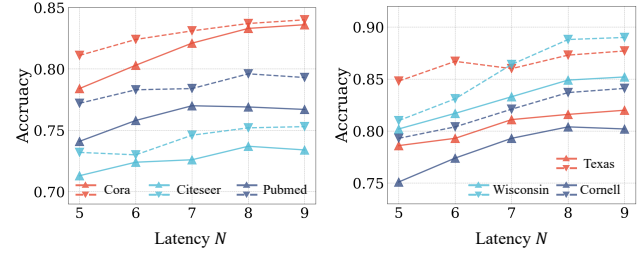


Figure 2. Sensitivity analysis on time latency N in SNNs across various datasets. The solid line denotes the results of COS-GNN-1st, and the dotted line denotes the COS-GNN-2nd.

and complexity, we set N to 8 as default.

6. Conclusion

In this paper, we address the practical problem of continuous spiking graph representation learning and propose an effective method named COS-GNN. COS-GNN integrates SNNs and CGNNs into a unified framework from two distinct time dimensions, thus retaining the benefits of low-power consumption and fine-grained feature extraction. Considering that the high-order structure would help to relieve the problem of information loss, we derive the second-order spike representation and investigate the backpropagation of second-order SNNs, and subsequently introduced the second-order COS-GNN. To ensure the stability of COS-GNN, we further prove that COS-GNN mitigates the gradient exploding and vanishing problem. Extensive experiments on diverse datasets validate the efficacy of proposed COS-GNN compared with various competing methods. In future work, we will explore the higher-order structure for more efficient continuous graph learning.

7. Impact Statements

This work introduces an innovative approach for continuous spiking graph neural network, with the objective of advancing the machine learning field, particularly in the domain of graph neural networks. The proposed method has the potential to substantially enhance the efficiency and scalability of graph learning tasks. The societal implications of this research are multifaceted. The introduced method has

the capacity to contribute to the development of more efficient and effective machine learning systems, with potential applications across various domains, including healthcare, education, and technology. Such advancements could lead to improved services and products, ultimately benefiting society as a whole.

References

Battaglia, P., Pascanu, R., Lai, M., Jimenez Rezende, D., et al. Interaction networks for learning about objects, relations and physics. *Proceedings of the Conference on Neural Information Processing Systems*, 2016.

Bellec, G., Salaj, D., Subramoney, A., Legenstein, R., and Maass, W. Long short-term memory and learning-to-learn in networks of spiking neurons. In *Proceedings of the Conference on Neural Information Processing Systems*, pp. 795–805, 2018.

Bohte, S., Kok, J., and La Poutre, H. Spikeprop: Backpropagation for networks of spiking neurons error-backpropagation in a network of spiking neurons. In *ESANN*, 2000.

Bresson, X. and Laurent, T. Residual gated graph convnets. *arXiv preprint arXiv:1711.07553*, 2017.

Brette, R., Rudolph, M., Carnevale, T., Hines, M., Beeman, D., Bower, J. M., Diesmann, M., Morrison, A., Goodman, P. H., Harris, F. C., et al. Simulation of networks of spiking neurons: a review of tools and strategies. *Journal of computational neuroscience*, 23:349–398, 2007.

Chamberlain, B., Rowbottom, J., Goranova, M. I., Bronstein, M., Webb, S., and Rossi, E. Grand: Graph neural diffusion. In *Proceedings of the International Conference on Machine Learning*, pp. 1407–1418, 2021.

Chen, M., Wei, Z., Huang, Z., Ding, B., and Li, Y. Simple and deep graph convolutional networks. In *Proceedings of the International Conference on Machine Learning*, pp. 1725–1735, 2020.

Chen, R. T., Rubanova, Y., Bettencourt, J., and Duvenaud, D. K. Neural ordinary differential equations. In *Proceedings of the Conference on Neural Information Processing Systems*, 2018.

Chien, E., Peng, J., Li, P., and Milenkovic, O. Adaptive universal generalized pagerank graph neural network. In *Proceedings of the International Conference on Learning Representations*, 2020.

Defferrard, M., Bresson, X., and Vandergheynst, P. Convolutional neural networks on graphs with fast localized spectral filtering. In *Proceedings of the Conference on Neural Information Processing Systems*, 2016.

Eshraghian, J. K., Ward, M., Neftci, E. O., Wang, X., Lenz, G., Dwivedi, G., Bennamoun, M., Jeong, D. S., and Lu, W. D. Training spiking neural networks using lessons from deep learning. *Proceedings of the IEEE*, 2023.

Esser, S. K., Appuswamy, R., Merolla, P., Arthur, J. V., and Modha, D. S. Backpropagation for energy-efficient neuromorphic computing. In *Proceedings of the Conference on Neural Information Processing Systems*, pp. 1117–1125, 2015.

Fey, M., Lenssen, J. E., Weichert, F., and Müller, H. Splinecnn: Fast geometric deep learning with continuous b-spline kernels. In *Proceedings of the IEEE/CVF Conference on Computer Vision and Pattern Recognition*, pp. 869–877, 2018.

Finzi, M. A., Bondesan, R., and Welling, M. Probabilistic numeric convolutional neural networks. In *Proceedings of the International Conference on Learning Representations*, 2021.

Gupta, J., Vemprala, S., and Kapoor, A. Learning modular simulations for homogeneous systems. In *Proceedings of the Conference on Neural Information Processing Systems*, pp. 14852–14864, 2022.

Hafiene, N., Karoui, W., and Romdhane, L. B. Influential nodes detection in dynamic social networks: A survey. *Expert Systems with Applications*, 159:113642, 2020.

Hairer, E., Norsett, S., and Wanner, G. *Solving Ordinary Differential Equations I: Nonstiff Problems*, volume 8. 01 1993. ISBN 978-3-540-56670-0. doi: 10.1007/978-3-540-78862-1.

Hamilton, W., Ying, Z., and Leskovec, J. Inductive representation learning on large graphs. In *Proceedings of the Conference on Neural Information Processing Systems*, 2017.

Hsieh, T.-Y., Wang, S., Sun, Y., and Honavar, V. Explainable multivariate time series classification: a deep neural network which learns to attend to important variables as well as time intervals. In *Proceedings of the International ACM Conference on Web Search & Data Mining*, pp. 607–615, 2021.

Hu, Y., Tang, H., and Pan, G. Spiking deep residual networks. *IEEE Transactions on Neural Networks and Learning Systems*, 2021.

Huang, Z., Sun, Y., and Wang, W. Learning continuous system dynamics from irregularly-sampled partial observations. In *Proceedings of the Conference on Neural Information Processing Systems*, volume 33, pp. 16177–16187, 2020.

Huang, Z., Sun, Y., and Wang, W. Coupled graph ode for learning interacting system dynamics. In *Proceedings of the International ACM SIGKDD Conference on Knowledge Discovery & Data Mining*, pp. 705–715, 2021.

Kim, S., Park, S., Na, B., and Yoon, S. Spiking-yolo: spiking neural network for energy-efficient object detection. In *Proceedings of the AAAI Conference on Artificial Intelligence*, pp. 11270–11277, 2020.

Kipf, T., Fetaya, E., Wang, K.-C., Welling, M., and Zemel, R. Neural relational inference for interacting systems. In *Proceedings of the International Conference on Machine Learning*, pp. 2688–2697, 2018.

Kipf, T. N. and Welling, M. Semi-supervised classification with graph convolutional networks. In *Proceedings of the International Conference on Learning Representations*, 2017.

LeCun, Y., Bottou, L., Bengio, Y., and Haffner, P. Gradient-based learning applied to document recognition. *Proceedings of the IEEE*, 86(11):2278–2324, 1998.

Li, J., Yu, Z., Zhu, Z., Chen, L., Yu, Q., Zheng, Z., Tian, S., Wu, R., and Meng, C. Scaling up dynamic graph representation learning via spiking neural networks. In *Proceedings of the AAAI Conference on Artificial Intelligence*, pp. 8588–8596, 2023.

Liao, S., Liang, S., Meng, Z., and Zhang, Q. Learning dynamic embeddings for temporal knowledge graphs. In *Proceedings of the International ACM Conference on Web Search & Data Mining*, pp. 535–543, 2021.

Luo, X., Yuan, J., Huang, Z., Jiang, H., Qin, Y., Ju, W., Zhang, M., and Sun, Y. Hope: High-order graph ode for modeling interacting dynamics. In *Proceedings of the International Conference on Machine Learning*, pp. 23124–23139, 2023.

Maass, W. Networks of spiking neurons: the third generation of neural network models. *Neural networks*, 10(9):1659–1671, 1997.

McCallum, A. K., Nigam, K., Rennie, J., and Seymore, K. Automating the construction of internet portals with machine learning. *Information Retrieval*, 3:127–163, 2000.

Meng, Q., Xiao, M., Yan, S., Wang, Y., Lin, Z., and Luo, Z.-Q. Training high-performance low-latency spiking neural networks by differentiation on spike representation. In *Proceedings of the IEEE/CVF Conference on Computer Vision and Pattern Recognition*, pp. 12444–12453, 2022.

Monti, F., Boscaini, D., Masci, J., Rodola, E., Svoboda, J., and Bronstein, M. M. Geometric deep learning on graphs and manifolds using mixture model cnns. In *Proceedings of the IEEE/CVF Conference on Computer Vision and Pattern Recognition*, pp. 5115–5124, 2017.

Namata, G., London, B., Getoor, L., Huang, B., and Edu, U. Query-driven active surveying for collective classification. In *10th International Workshop on Mining and Learning with Graphs*, volume 8, pp. 1, 2012.

Pei, H., Wei, B., Chang, K. C.-C., Lei, Y., and Yang, B. Geom-gcn: Geometric graph convolutional networks. *arXiv preprint arXiv:2002.05287*, 2020.

Poli, M., Massaroli, S., Park, J., Yamashita, A., Asama, H., and Park, J. Graph neural ordinary differential equations. *arXiv preprint arXiv:1911.07532*, 2019.

Rathi, N., Srinivasan, G., Panda, P., and Roy, K. Enabling deep spiking neural networks with hybrid conversion and spike timing dependent backpropagation. In *Proceedings of the International Conference on Machine Learning*, 2020.

Rueckauer, B., Lungu, I.-A., Hu, Y., Pfeiffer, M., and Liu, S.-C. Conversion of continuous-valued deep networks to efficient event-driven networks for image classification. *Frontiers in neuroscience*, 11:682, 2017.

Rusch, T. K., Chamberlain, B., Rowbottom, J., Mishra, S., and Bronstein, M. Graph-coupled oscillator networks. In *Proceedings of the International Conference on Machine Learning*, pp. 18888–18909, 2022.

Sen, P., Namata, G., Bilgic, M., Getoor, L., Galligher, B., and Eliassi-Rad, T. Collective classification in network data. *AI magazine*, 29(3):93–93, 2008.

Velickovic, P., Cucurull, G., Casanova, A., Romero, A., Lio, P., Bengio, Y., et al. Graph attention networks. In *Proceedings of the International Conference on Learning Representations*, 2017.

Wu, F., Souza, A., Zhang, T., Fifty, C., Yu, T., and Weinberger, K. Simplifying graph convolutional networks. In *Proceedings of the International Conference on Machine Learning*, pp. 6861–6871, 2019.

Xhonneux, L.-P., Qu, M., and Tang, J. Continuous graph neural networks. In *Proceedings of the International Conference on Machine Learning*, 2020.

Xu, K., Hu, W., Leskovec, J., and Jegelka, S. How powerful are graph neural networks? In *Proceedings of the International Conference on Learning Representations*, 2019.

Zhang, D., Zhang, T., Jia, S., Wang, Q., and Xu, B. Recent advances and new frontiers in spiking neural networks. In *Proceedings of the International Joint Conference on Artificial Intelligence*, pp. 5670–5677, 2022a.

Zhang, Y., Gao, S., Pei, J., and Huang, H. Improving social network embedding via new second-order continuous graph neural networks. In *Proceedings of the International ACM SIGKDD Conference on Knowledge Discovery & Data Mining*, pp. 2515–2523, 2022b.

Zhao, L. and Akoglu, L. Pairnorm: Tackling oversmoothing in gnns. *arXiv preprint arXiv:1909.12223*, 2019.

Zhu, J., Yan, Y., Zhao, L., Heimann, M., Akoglu, L., and Koutra, D. Generalizing graph neural networks beyond homophily. In *Proceedings of the Conference on Neural Information Processing Systems*, 2020.

Zhu, Z., Peng, J., Li, J., Chen, L., Yu, Q., and Luo, S. Spiking graph convolutional networks. In *Proceedings of the International Joint Conference on Artificial Intelligence*, pp. 2434–2440, 2022.

A. Proof of Proposition 4.1

Proposition 4.1 Define the first-order SNNs ODE as $\frac{du_t^\tau}{d\tau} = g(u_t^\tau, \tau)$, and first-order Graph ODE as $\frac{du_t^\tau}{dt} = f(u_t^\tau, t)$, then the first-order graph PDE network can be formulated as:

$$u_{t+1}^{\tau+1} = u_0^0 + \int_0^T f \left(u_y^0 + \int_0^N g(u_y^x, x) dx \right) dy + \int_0^N g \left(u_0^x + \int_0^{T-1} f(u_y^x, y) dy \right) dx.$$

Proof.

$$\frac{du_t^\tau}{d\tau} = g(u_t^\tau, \tau), \quad \frac{du_t^\tau}{dt} = f(u_t^\tau, t),$$

u_t^τ is a function related to variable t and τ , we have $\frac{\partial u_t^\tau}{\partial \tau} = g(u_t^\tau, \tau)$ and $\frac{\partial u_t^\tau}{\partial t} = f(u_t^\tau, t)$. Thus,

$$u_t^{\tau+1} = u_t^\tau + \int_\tau^{\tau+1} g(u_t^x, x) dx, \quad u_{t+1}^{\tau+1} = u_t^{\tau+1} + \int_t^{\tau+1} f(u_y^{\tau+1}, y) dy, \quad (15)$$

$$\begin{aligned} u_T^N &= u_{T-1}^{N-1} + \int_{T-1}^T f(u_y^N, y) dy + \int_{N-1}^N g(u_{T-1}^x, x) dx \\ &= u_{T-2}^{N-2} + \int_{T-2}^T f(u_y^N, y) dy + \int_{N-2}^N g(u_{T-1}^x, x) dx \\ &= u_0^0 + \int_0^T f(u_y^N, y) dy + \int_0^N g(u_{T-1}^x, x) dx \\ &= u_0^0 + \int_0^T f \left(u_y^{N-1} + \int_{N-1}^N g(u_y^x, x) dx \right) dy + \int_0^N g \left(u_{T-2}^x + \int_{T-2}^{T-1} f(u_y^x, y) dy \right) dx \\ &= u_0^0 + \int_0^T f \left(u_y^0 + \int_0^N g(u_y^x, x) dx \right) dy + \int_0^N g \left(u_0^x + \int_0^{T-1} f(u_y^x, y) dy \right) dx. \end{aligned} \quad (16)$$

By adding the initial state on each time step and latency with $u_0^0 = 0$ and $u_0^\tau = 0$, we have:

$$\begin{aligned} u_T^N &= \int_0^T f \left(\int_0^N g(u_y^x, x) dx \right) dy + \int_0^N g \left(\int_0^{T-1} f(u_y^x, y) dy \right) dx \\ &= \underbrace{\int_0^{T-1} f \left(\int_0^N g(u_y^x, x) dx \right) dy}_{\text{first term}} + \underbrace{\int_0^N g \left(\int_0^{T-1} f(u_y^x, y) dy \right) dx + \int_{T-1}^T f \left(\int_0^N g(u_y^x, x) dx \right) dy}_{\text{second term}} \\ &= 2 \int_0^{T-1} f \left(\int_0^N g(u_y^x, x) dx \right) dy + \int_{T-1}^T f \left(\int_0^N g(u_y^x, x) dx \right) dy. \end{aligned} \quad (17)$$

The first term denotes that the SNNs and CGNNs are interactively updated during the time step 0 to $T-1$, and the second term denotes that at the last time step T , COS-GNN simply calculates the CGNNs process while ignoring the SNNs for prediction.

B. Proof of Eqn. 11

Proof. From Eq. 9, we have:

$$u(\tau+1) = \beta^2 u(\tau-k+1) + \alpha \sum_{i=0}^{k-1} \beta^i I_{syn}(\tau-i) + \sum_{i=0}^{k-1} \beta^i (I_{input}(\tau-i) - V_{th}s(\tau-i)), \quad (18)$$

$$u(N) = \alpha \sum_{n=0}^{N-1} \beta^n I_{syn}(N-n-1) + \sum_{n=0}^{N-1} \beta^n (I_{input}(N-n-1) - V_{th}s(N-n-1)). \quad (19)$$

Due to:

$$I_{syn}(\tau + 1) = \alpha^k I_{syn}(\tau - k + 1) + \sum_{i=0}^k \alpha^i I_{input}(\tau - i), \quad (20)$$

we have,

$$\begin{aligned} u(N) &= \alpha \sum_{n=0}^{N-1} \beta^{N-n-1} I_{syn}(n) + \sum_{n=0}^{N-1} \beta^{N-n-1} (I_{input}(n) - V_{th}s(n)) \\ &= \alpha \left(\left(\frac{\beta^{N-1} \alpha^{-1} \left(1 - \left(\frac{\alpha}{\beta} \right)^N \right)}{1 - \frac{\alpha}{\beta}} \right) I_{in}(0) + \left(\frac{\beta^{N-2} \alpha^{-1} \left(1 - \left(\frac{\alpha}{\beta} \right)^{N-1} \right)}{1 - \frac{\alpha}{\beta}} \right) I_{in}(1) + \dots \right. \\ &\quad \left. + \left(\frac{\beta^{N-i} \alpha^{-1} \left(1 - \left(\frac{\alpha}{\beta} \right)^{N-i+1} \right)}{1 - \frac{\alpha}{\beta}} \right) I_{in}(i-1) + \dots + (\beta^2 \alpha^{-1} + \beta + \alpha) I_{in}(N-3) \right. \\ &\quad \left. + (\beta \alpha^{-1} + 1) I_{in}(N-2) + \alpha^{-1} I_{in}(N-1) \right) - \sum_{n=0}^{N-1} \beta^{N-n-1} V_{th}s(n) \\ &= \frac{1}{\beta - \alpha} \left(\left(\beta^N \left(1 - \left(\frac{\alpha}{\beta} \right)^N \right) I_{in}(0) \right) + \dots + \left(\beta^{N-i+1} \left(1 - \left(\frac{\alpha}{\beta} \right)^{N-i+1} \right) I_{in}(i-1) \right) \right. \\ &\quad \left. + \dots + (\beta - \alpha) I_{in}(N-1) \right) - \sum_{n=0}^{N-1} \beta^{N-n-1} V_{th}s(n) \\ &= \frac{1}{\beta - \alpha} \sum_{n=0}^{N-1} (\beta^{N-n} - \alpha^{N-n}) I_{in}(n) - \sum_{n=0}^{N-1} \beta^{N-n-1} V_{th}s(n). \end{aligned}$$

Define $\hat{I}(N) = \frac{1}{(\beta - \alpha)^2} \frac{\sum_{n=0}^{N-1} (\beta^{N-n} - \alpha^{N-n}) I_{in}(n)}{\sum_{n=0}^{N-1} (\beta^{N-n} - \alpha^{N-n})}$, and $\hat{a}(N) = \frac{1}{\beta^2} \frac{V_{th} \sum_{n=0}^{N-1} \beta^{N-n} s(n)}{\sum_{n=0}^{N-1} (\beta^{N-n} - \alpha^{N-n})}$, we have:

$$\hat{a}(N) = \frac{\beta - \alpha}{\beta} \frac{\hat{I}(N)}{\Delta \tau} - \frac{u(N)}{\Delta \tau \beta \sum_{n=0}^{N-1} (\beta^{N-n} - \alpha^{N-n})} \approx \frac{\tau_{syn} \tau_{mem}}{\tau_{mem} - \tau_{syn}} \hat{I}(N) - \frac{u(N)}{\Delta \tau \beta \sum_{n=0}^{N-1} (\beta^{N-n} - \alpha^{N-n})},$$

where $\alpha = \exp(-\Delta \tau / \tau_{syn})$, $\beta = \exp(-\Delta \tau / \tau_{mem})$.

C. Proof of Proposition 4.3

Proposition 4.3 Define the second-order SNNs as $\frac{d^2 u_t^\tau}{d\tau^2} + \delta \frac{du_t^\tau}{d\tau} = g(u_t^\tau, \tau)$, and second-order CGNNs as $\frac{d^2 u_t^\tau}{dt^2} + \gamma \frac{du_t^\tau}{dt} = f(u_t^\tau, t)$, then the second-order COS-GNN is formulated as:

$$u_t^\tau = \int_0^T h \left(\int_0^N e(u_t^\tau) d\tau \right) dt = \int_0^N e \left(\int_0^T h(u_t^\tau) dt \right) d\tau,$$

$$\frac{\partial^2 u_t^\tau}{\partial \tau^2} + \delta \frac{\partial u_t^\tau}{\partial \tau} = g(u_t^\tau), \quad \frac{\partial^2 u_t^\tau}{\partial t^2} + \gamma \frac{\partial u_t^\tau}{\partial t} = f(u_t^\tau),$$

where $e(u_t^\tau) = \int_0^N g(u_t^\tau) d\tau - \delta(u_t^N - u_t^0)$, and $h(u_t^\tau) = \int_0^T f(u_t^\tau) dt - \gamma(u_T^\tau - u_0^\tau)$.

Proof. Obviously,

$$\frac{\partial^2 u_t^\tau}{\partial \tau^2} + \delta \frac{\partial u_t^\tau}{\partial \tau} = g(u_t^\tau), \quad \frac{\partial^2 u_t^\tau}{\partial t^2} + \gamma \frac{\partial u_t^\tau}{\partial t} = f(u_t^\tau),$$

$$so, \quad \frac{\partial u_t^\tau}{\partial \tau} + \delta(u_t^N - u_t^0) = \int_0^N g(u_t^\tau) d\tau, \quad \frac{\partial u_t^\tau}{\partial t} + \gamma(u_T^\tau - u_0^\tau) = \int_0^T f(u_t^\tau) dt.$$

Define $e(u_t^\tau) = \int_0^N g(u_t^\tau) d\tau - \delta(u_t^N - u_t^0)$, and $h(u_t^\tau) = \int_0^T f(u_t^\tau) dt - \gamma(u_T^\tau - u_0^\tau)$, we have:

$$\frac{\partial u_t^\tau}{\partial \tau} = e(u_t^\tau), \quad \frac{\partial u_t^\tau}{\partial t} = h(u_t^\tau),$$

thus,

$$u_t^\tau = \int_0^T h\left(\int_0^N e(u_t^\tau) d\tau\right) dt = \int_0^N e\left(\int_0^T h(u_t^\tau) dt\right) d\tau,$$

where $\frac{\partial e(u_t^\tau)}{\partial \tau} = g(u_t^\tau)$ and $\frac{\partial h(u_t^\tau)}{\partial t} = f(u_t^\tau)$.

D. Proof of Proposition 4.4

Proposition 4.4 *Let \mathbf{X}^n and \mathbf{Y}^n be the node features, generated by Eqn. 3, and $\Delta t \ll 1$. The gradient of the second-order CGNNs \mathbf{W}_l is bounded as Eqn. 21, and the gradient of the second-order SNNs \mathbf{W}^k is bounded as Eqn. 22:*

$$\left| \frac{\partial \mathcal{L}}{\partial \mathbf{W}_l} \right| \leq \frac{\beta' \hat{\mathbf{D}} \Delta t (1 + \Gamma T \Delta t)}{v} \left(\max_{1 \leq i \leq v} (|\mathbf{X}_i^0| + |\mathbf{Y}_i^0|) \right) + \frac{\beta' \hat{\mathbf{D}} \Delta t (1 + \Gamma T \Delta t)}{v} \left(\max_{1 \leq i \leq v} |\bar{\mathbf{X}}_i| + \beta \sqrt{T \Delta t} \right)^2, \quad (21)$$

$$\left| \frac{\partial \mathcal{L}}{\partial \mathbf{W}^k} \right| \leq \frac{(1 + T \Gamma \Delta t)(1 + N \Theta \Delta \tau) V_{th}}{v \beta^2 \Delta \tau} \left(\max_{1 \leq i \leq v} |\mathbf{X}_i^N| + \max_{1 \leq i \leq v} |\bar{\mathbf{X}}_i| \right). \quad (22)$$

where $\beta = \max_x |\sigma(x)|$, $\beta' = \max_x |\sigma'(x)|$, $\hat{D} = \max_{i,j \in \mathcal{V}} \frac{1}{\sqrt{d_i d_j}}$, and $\Gamma := 6 + 4\beta' \hat{D} \max_{1 \leq n \leq T} \|\mathbf{W}^n\|_1$, $\Theta := 6 + 4\beta' \hat{D} \max_{1 \leq n \leq N} \|\mathbf{W}^n\|_1$. d_i is the degree of node i , $\bar{\mathbf{X}}_i$ is the label of node i .

$$\begin{aligned} \frac{\partial \mathcal{L}}{\partial \mathbf{W}^k} &= \frac{\partial \mathcal{L}}{\partial \mathbf{Z}_T^N} \frac{\partial \mathbf{Z}_T^N}{\partial \mathbf{Z}_l^N} \frac{\partial \mathbf{Z}_l^N}{\partial \mathbf{W}^k} = \frac{\partial \mathcal{L}}{\partial \mathbf{Z}_T^N} \prod_{n=l+1}^T \frac{\partial \mathbf{Z}_n^N}{\partial \mathbf{Z}_{n-1}^N} \frac{\partial \mathbf{Z}_l^N}{\partial \mathbf{W}^k} \\ &= \frac{\partial \mathcal{L}}{\partial \mathbf{Z}_T^N} \prod_{n=l+1}^T \frac{\partial \mathbf{Z}_n^N}{\partial \mathbf{Z}_{n-1}^N} \frac{\partial \mathbf{Z}_l^N}{\partial \mathbf{Z}_l^k} \frac{\partial \mathbf{Z}_l^k}{\partial \mathbf{W}^k} \\ &= \frac{\partial \mathcal{L}}{\partial \mathbf{Z}_T^N} \prod_{n=l+1}^T \frac{\partial \mathbf{Z}_n^N}{\partial \mathbf{Z}_{n-1}^N} \prod_{i=k+1}^N \frac{\partial \mathbf{Z}_i^N}{\partial \mathbf{Z}_l^{i-1}} \frac{\partial \mathbf{Z}_l^k}{\partial \mathbf{W}^k}, \end{aligned}$$

From (Rusch et al., 2022), we have:

$$\left\| \frac{\partial \mathcal{L}}{\partial \mathbf{Z}_T^N} \right\|_\infty \leq \frac{1}{v} \left(\max_{1 \leq i \leq v} |\mathbf{X}_i^N| + \max_{1 \leq i \leq v} |\bar{\mathbf{X}}_i| \right), \quad \left\| \frac{\partial \mathbf{Z}_T^N}{\partial \mathbf{Z}_t^N} \right\|_\infty \leq 1 + T \Gamma \Delta t. \quad (23)$$

Due to the second-order SNN has a similar formulation to second-order GNN, we have a similar conclusion,

$$\left\| \frac{\partial \mathbf{Z}_l^N}{\partial \mathbf{Z}_l^k} \right\|_\infty \leq 1 + N \Theta \Delta \tau, \quad (24)$$

with $\beta = \max_x |\sigma(x)|$, $\beta' = \max_x |\sigma'(x)|$, $\hat{D} = \max_{i,j \in \mathcal{V}} \frac{1}{\sqrt{d_i d_j}}$, and $\Theta := 6 + 4\beta' \hat{D} \max_{1 \leq n \leq N} \|\mathbf{W}^n\|_1$, and with Eq. 12, we have:

$$\frac{\partial \mathbf{Z}_l^k}{\partial \mathbf{W}^k} \approx r(\mathbf{Z}_l^{k-1}) \leq \frac{V_{th}}{\beta^2 \Delta \tau}. \quad (25)$$

Multipling 23, 24 and 25, we have the upper bound:

$$\frac{\partial \mathcal{L}}{\partial \mathbf{W}^k} \leq \frac{(1 + T \Gamma \Delta t)(1 + N \Theta \Delta \tau) V_{th}}{v \beta^2 \Delta \tau} \left(\max_{1 \leq i \leq v} |\mathbf{X}_i^N| + \max_{1 \leq i \leq v} |\bar{\mathbf{X}}_i| \right). \quad (26)$$